REPORT DOCUMENTATION PAGE

AFRL-SR-BL-TR-00-

$0\varphi\varphi1$

9

1. AGENCY USE ONLY *(Leave blank)*	2. REPORT DATE 08-05-00	3. ~~REPORT TYPE AND DATES~~ COVERED Final Report 01 June 1996 - 01 May 1999

4. TITLE AND SUBTITLE

SHEAR WAVE GENERATION FROM OVERDRIVEN CAVITIES IN ROCK

5. FUNDING NUMBERS

AFOSR Grant F49620-96-1-0208

6. AUTHOR(S)

Charles Cangli Liu & Thomas J. Ahrens

7. PERFORMING ORGANIZATION NAME(S) AND ADDRESS(ES)

CALIFORNIA INSTITUTE OF TECHNOLOGY

Seismological Laboratory 252-21

1200 E. California Blvd.

Pasadena, CA 91125

8. PERFORMING ORGANIZATION REPORT NUMBER

9. SPONSORING/MONITORING AGENCY NAME(S) AND ADDRESS(ES)

AFORSR

AASERT Program

801 N. Randolph St., Rm 732

Arlington, VA 22203-1977

10. SPONSORING/MONITORING AGENCY REPORT NUMBER

11. SUPPLEMENTARY NOTES

12a. DISTRIBUTION AVAILABILITY STATEMENT

Approved for public release: Distribution Unlimited

12b. DISTRIBUTION CODE

13. ABSTRACT *(Maximum 200 words)*

During the period of this award, the basic structure-based model for rapid distortions of homogeneous turbulence was extended to deal with slow distortions and inhomegeneities. A computer program was written to study the extended model in free-serar flows. The model was installed in NASA's INS2D code for generalized flow analysis. Mr. Maire carried out this work as part of his Phi) research. During the award period we began to explore ways to simplify the structure-based modeling so that it could be used in repetitive engineering calculations. The idea is to use an algebraic version of the model that, gives the turbulent, streses in terms of the mean strain rate and mean and frame rotation rates as an alternative to the linear or non linear s/res strain relationships used in conventional two equation modeling. The difference would be that the algebraic structure-based turbulence model (ASBM) would do a much better job of representing the streses in complex flows. Development of this concept into a working engineerhag model and codes will be the principal objective under subsequent awards.

DTIC QUALITY INSPECTED 4

20001208 065

14. SUBJECT TERMS SHEAR WAVE GENERATION FROM OVERDRIVEN CAVITIES IN ROCK			15. NUMBER OF PAGES
			16. PRICE CODE

17. SECURITY CLASSIFICATION OF REPORT	18. SECURITY CLASSIFICATION OF THIS PAGE	19. SECURITY CLASSIFICATION OF ABSTRACT	20. LIMITATION OF ABSTRACT
UNCLASSIFIED	UNCLASSIFIED	UNCLASSIFIED	

Shear Wave Generation from Overdriven Cavities in Rock

Final Report

Charles Cangli Liu and Thomas J. Ahrens

California Institute of Technology
Pasadena, CA   91125

Table of Contents

Cover Page
Standard Form 298 (includes abstract)

2

List of Illustrations

List of Tables

1. Status of Effort

We have developed a measurement method to monitor P- and S-waves generated from small laboratory scale explosions in meter-sized rock media, at a series of stations. We have also invented an unique device to drill spherical cavities in rocks to explore the nature of seismic radiation from nearly spherically symmetric centrally-placed explosive charges in rock.

Laboratory explosive experiments in which the P- and S- body waves are generated from explosive charges detonated within rock cavities are compared to seismic radiation from tensional fracture of the medium surrounding spherical and cylindrical symmetry charges that were detonated at the center of cavities in rock. The records and post-explosion studies of the experiments are consistent with, but do not prove, ideas currently being evaluated for brittle media which suggest that "failure waves" (FW) propagating at less than shear wave velocity could provide a microscopic model of brittle failure. The FW separate region that is damaged from still intact material. The experiments verify that the S-waves are generated from both P- to S-wave conversion on the cavity wall and quite separately, from cracking in rocks. We have previously analyzed P- and S-waves produced by explosions in rock cavities and radial cracking which occurs when the cavity is overdriven. The predications of the model fit our observations qualitatively. A theoretical model is proposed to explain the differences on P-wave induced displacement history between the observed and theoretical spherical pulse wave models. Using the measured displacement decay relation and the dynamic tensile and shear strength, a simple strength model is derived to estimate the S-wave amplitude generated from P- to S-wave conversion and rock cracking. The magnitudes of the S-wave amplitude obtained from the strength of material models are in good agreement with the experimental results. The present results demonstrated the important role of rock cracking in shear wave generation and the modification of P-wave profile in overdriven rock cavities. The results from this work need to be scaled and tested for larger explosive charges and recorded over longer propagation distances. The rich phenomena associated with waves generated from underground explosions in cavities indicate that this research direction will provide new criteria for relating in-situ stress and preferred cleavage at possible explosive test sites. If these data are understood in detail, it appears that they may also be used to assist in the discrimination of earthquakes from explosions. Moreover, intrinsic differences in the signal from explosive gas-driven hydrofractures versus nuclear explosive-induced fracture of rock with a source that is deficient in gas may allow seismic discrimination of nuclear from chemical explosive sources.

2. Accomplishments/New Findings

Our objective is to understand the generation of shear waves from explosion in cavities. We have studied explosive sources and the effect of the relative orientation of cavity walls and the direction to the seismic receiver (transducer) in small scale models. Fracture dynamics plays an important role in the generation of s-waves when an explosive charge is detonated in overdriven cavity in our experiments having static pressures of 140-700 bars. In these experiments which were conducted within uniform rock material, Bedford limestone, which is used for building construction, the experimental assemblies were conducted within 30 to 150 cm cylindrical rock samples. The entire experiment including the rock, the explosive charges and the transducers which detected stress waves were encapsulated in plastic film and pressurized to approximately 8 atm hydrostatic pressure.

A complete pressurized container holding the rock sample, an electronic recording system, techniques for centrally emplacing a spherical charge (Figs. 1-2) within an emplacement (not two hemi-spherical charges cemented in place as in earlier experimental studies) were developed. We were able to record via a series of surface strain gauges, the P- and S-wave signals. Also fired were two tests which compare the spherical experiments with cylindrical geometry experiments (Fig. 3).
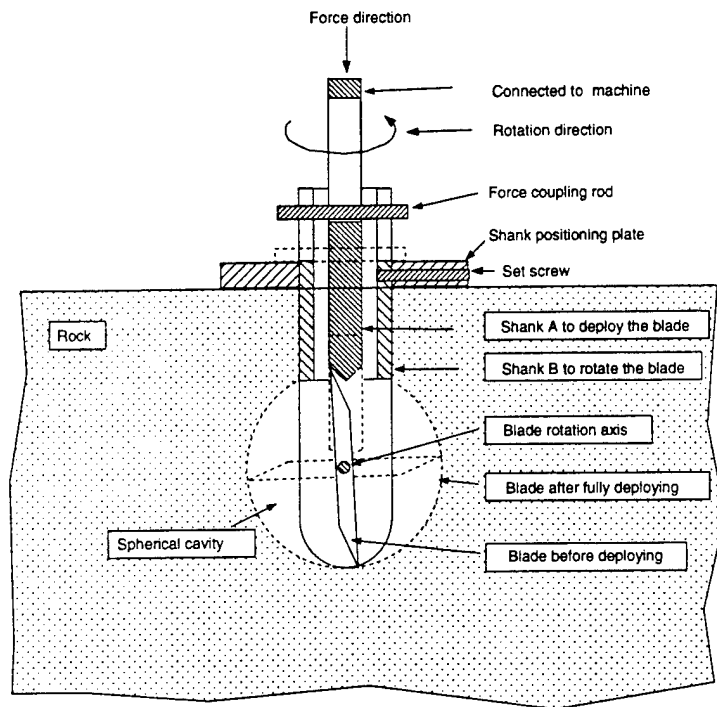

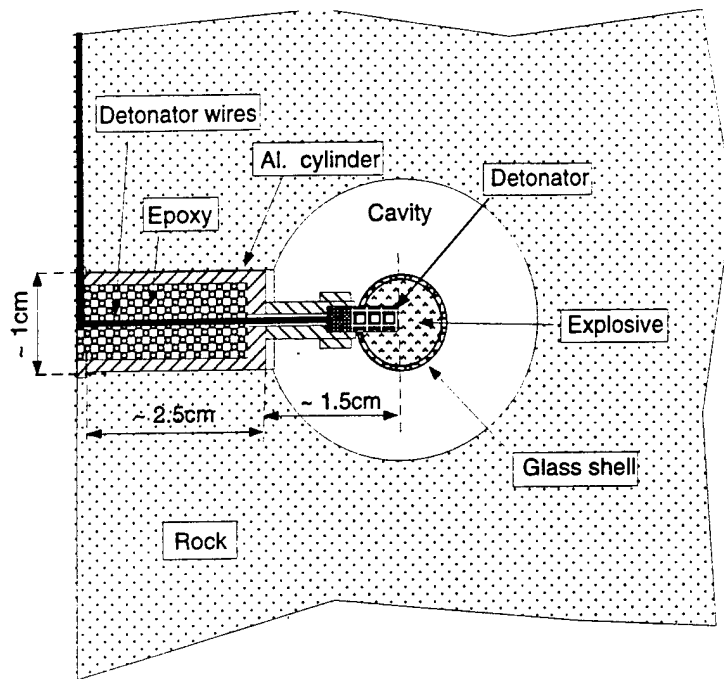Fig. 1. Schematic of spherical cavity drill

6

Fig. 2. Spherical explosive source arrangement.

In these experiments we fired a series of 0.4 to 1.9 gram charge PETN in cylindrical and spherical cavities (see Tables 1 and 2). Notably we observed the shear wave induced by rock cracking arrived at the transducers before the shear wave induced by mode conversion at the explosive cavity-wall rock interface.

We developed a generalized analytic model that describes the P- and S-waves from the shock-induced radial cracking. In this mode, we assume that the pressure history is divided into three time periods. These are: the reverberation dominated period, the cracking dominated period and a steady period. The reverberation model predicts a pressure profile which is calculated using the thermodynamic properties of the explosive product gases (see gauges #2 and 4, Figs. 4-5).

Table 1: Data for cylindrical cavity experiments

Shot #		Dimensions of explosive	Mass of explosive gram	Type of explosive	Dimensions of cavity	Theoretical Final Cavity Pressure (bar)
SW1	decoupled	ϕ 5 x6 mm	0.24	Pellet pressed PETN	ϕ30 x 30 mm	55
SW2	tamped	ϕ10x10mm	1.2	Data sheet PETN	ϕ 12x12 mm	4420

7

Strain gauges (7, 8)

Reflected SV- or
P-wave

Reflected P- or
SV-wave

5, 6

θ

3, 4

θ

1, 2

Incident P- or
SV-wave

Rock joint

61 cm

Explosives

Rock sample

30.5 cm
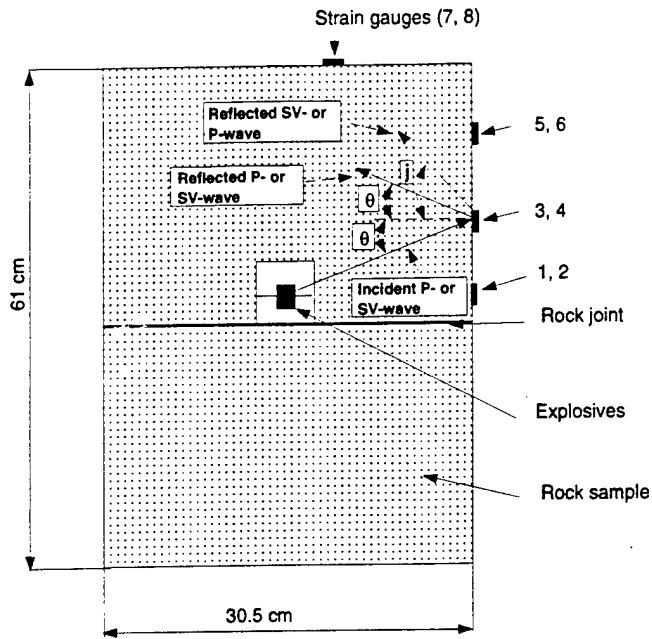
(A)   Layout of rock sample, strain gauges and explosive charge

Gauge 8

7

6

5

4

3

2

1

Direction 1

u_{per}

Direction 2 (u_{par})
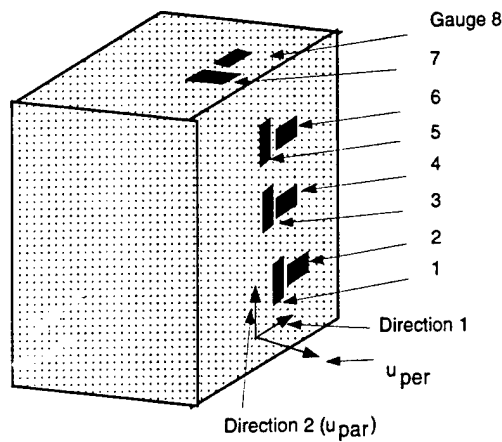
(B)   Sketch of polarization directions of strain gauges

Fig. 3. Sample and strain gauge layout for cylindrical cavity experiments. The strain gauge-explosive distances are given in Table 3.

Table 2. Data for spherical cavity experiments

Shot number	Explosive mass (gram)	Theoretical Final Cavity Pressure (bar)
SW4	1.9	675
SW5*	0.4	142
SW6*	0.6	213
SW7*	0.7	248
SW8*	0.8	284
SW9	0.8	284

Table 3. The distance between gauges and cavity center

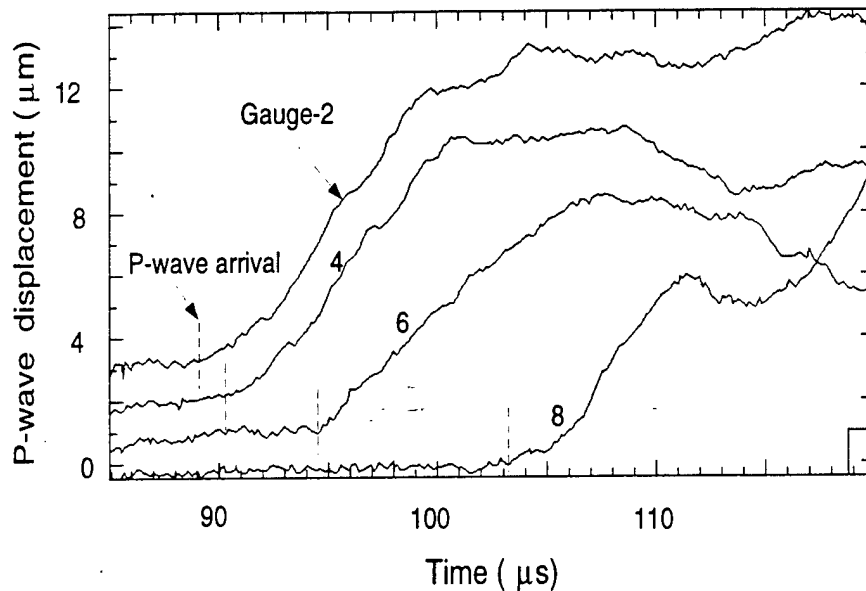| Shot number	Gauge 1&2	Gauge 3&4	Gauge 5&6	Gauge 7&8
SW1	152.9	156.9	186.7	238.0
SW2	153.0	161.6	197.6	241.6
SW4	152.3	157.8	174.3	208.9
SW9	152.2	158.0	180.1	214.0

Distance unit is mm.

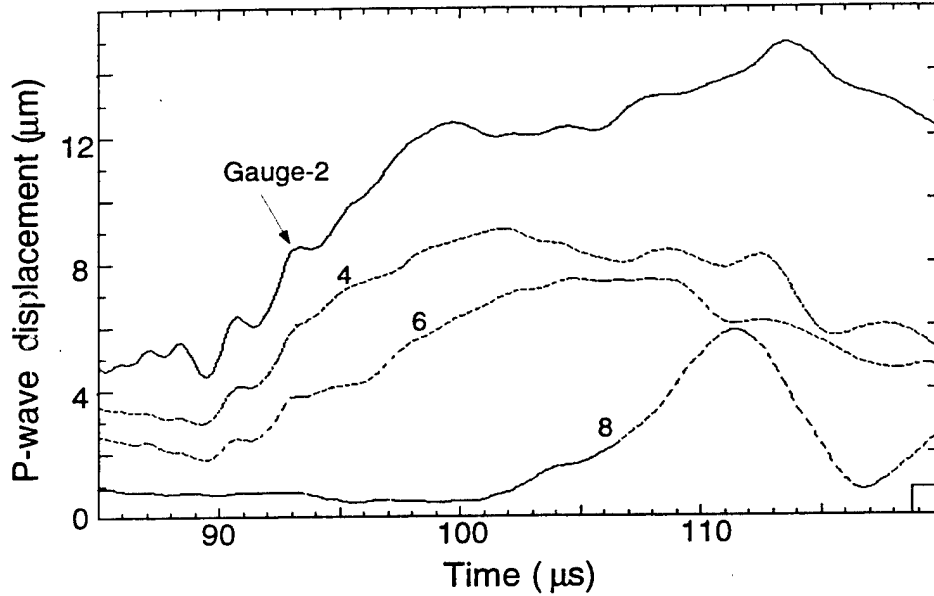Fig. 4. P-wave particle displacement versus time for SW4.

9

Fig. 5. P-wave particle displacement versus time for SW9.

The crack dominated period which we assume is induced by the nucleation of new cracks and growth of existing cracks during the time that the P-wave is propagating through the sample. These may represent the so-called failure wave recognized recently in glasses. Previously present macro-cracks are also activated by the P wave if stress related with P-wave is sufficient to induce tensional stresses higher than the local tensional strength and we think these give the most coherent S-wave signals. These start from the cavity wall and propagate into the rock. Macro-crack propagation is controlled by fracture dynamics. In this part, only the P-wave generated from macro-cracking is considered because P-waves generated from micro-cracks cannot be separated from the initial P-waves. When pressure in cavities is larger than some critical value, radial cracks are generated from inner surfaces. The tangential stresses in rock change during cracking because the tangential stress is tensional before cracking and compressional after cracking. Radial cracking generates P-waves because this thin form of cracking is equivalent to increasing the radius of the cavity.

3. Particle displacement induced by P-waves

The P-wave particle displacement is shown in Fig. 4 (shot SW4). From Figures 4 and 5, the maximum P-wave particle displacements, u_{max}, at different distances from the cavity center can be obtained and are shown in Fig. 6 in which Cowboy data are plotted. The experimental data is fit by

$$u_{max} = 1.32 \times 10^4 r^{-1.46}, \text{ for SW4}$$

$$u_{max} = 1.93 \times 10^4 r^{-1.56}, \text{ for SW9}$$

where u_{max}, is in $\hat{E}$m, r in mm is the distance from the cavity center. In Murphey's [1961] paper, he found that the field results have a dependence of the peak P-wave particle displacement on the distance from the cavity center that is proportional to $r^{-1.5}$. Thus, the previous study is very comparable with the results from this work.
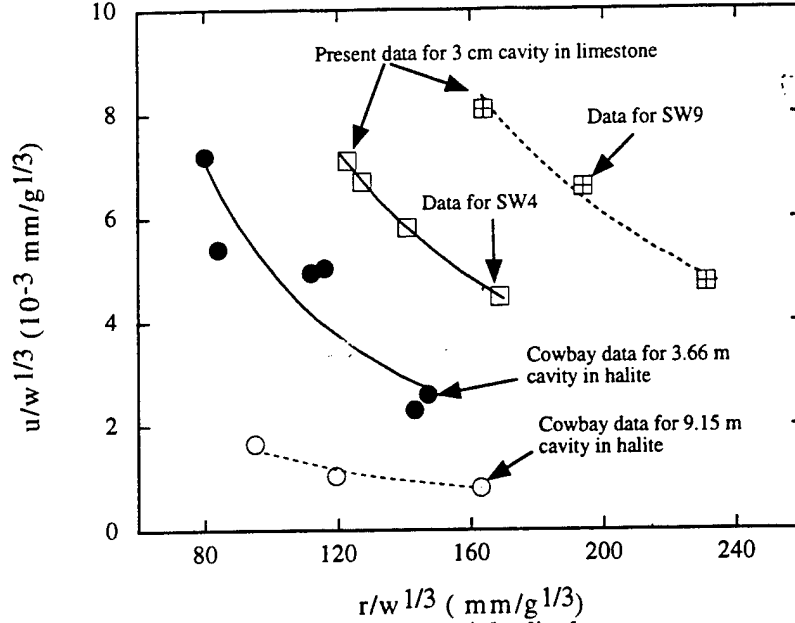
Fig. 6. Scaled maximum P-wave particle displacement versus propagation distance.

4. Comparison between experimental data and theoretical predictions.

The analytic solution for a pulsed spherical wave generated from an explosion in a spherical cavity is given by Timoshenko and Goodier [1970] as:

$$u = \frac{f'}{C_e r} + \frac{f}{r^2}, \tag{1}$$

where f is the solution of

$$f''(t) + 2\gamma f'(t) + \frac{2\gamma C_e}{a} f(t) = \frac{ap(t)}{\rho} \tag{2}$$

where γ (which has units of t^{-1}) is

$$\gamma = \frac{(1-2v)C_e}{(1-v)\ a} \tag{3}$$

where v is Poisson's ratio, u is particle displacement, C_e is P-wave velocity, is the radius of the cavity, p is gas pressure and p is P is gas density.

The particular solution of Eq. (2) for an outgoing wave from a spherical source [Timoshenko and Goodier, 1970] is

$$f(t) = \frac{1}{\alpha - \beta} \frac{a}{\rho} \int_0^t p(\tau)(e^{\alpha_0(t-\tau)} - e^{\beta_0(t-\tau)}) d\tau, \tag{4}$$

where

$$\alpha_0 = \gamma(-1+is), \tag{5}$$

$$\beta_0 = \gamma(-1-is), \tag{6}$$

$\tau = t-(r-a)/C_e$ and $s=(1-2v)^{-0.5}$.

If a step-like pressure history, i.e., $p(t)-p_0 H(t)$, is assumed, the particular solution [Timoshenko and Goodier, 1970] is

$$f(\tau) = \frac{p_0 a^2}{2\rho\gamma C_e} (1 - e^{\gamma\tau}(\cos(\gamma s\tau) + \frac{\sin(\gamma s\tau)}{s}),$$

The displacement history at r is [Timoshenko and Goodier, 1970]

11

$$u(t,r) = \frac{A}{r^2} + \frac{A}{C_e} \frac{Ae^{-\gamma\pi}}{r} ((\gamma s + \frac{\gamma}{s} - \frac{C_e}{rs}) \sin(\gamma s\tau) - \frac{C_e \cos(\gamma s\tau)}{r}, \quad (8)$$

where $A = p_0 a^2/(2\rho\gamma C_e)$.

The first term in the solution corresponds to the static solution, the second is dynamic term. The typical displacement history from Eq. 8 is shown in Fig 7 in which the experimental data from Shot SW1 fired in a cylindrical cavity using 0.24 g of explosive. We calculated that in this experiment the post detonation pressure was 55 bars. We assume this shot was decoupled. From this figure, we can see that the solution from only a pure spherical pulse can approximately explain the observed results obtained from an overdriven spherical cavities such as SW4 and SW9 (Table 2). There are, however, significant differences between the model and the observed displacements.
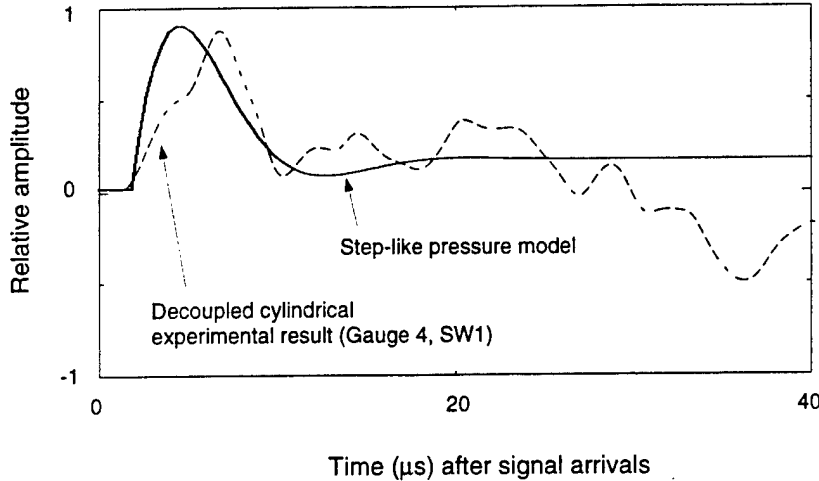
Fig. 7. Displacement - time history calculated from a step-like increase in pressure versus that observed on Gauge #4, SW1.

Fig. 8. Pressure history (a) crack velocity constant (b) crack velocity decreases with time.

The reasons for the difference may include:

1. The pressure history in cavity is not a single-step-like function. Because of the large mismatch of impedances between gas in cavity and rocks, shock waves generated by explosions in cavity generally reverberate several times before the pressure in cavity reaches

12

its final value. This means that the pressure history in cavity may have a multi-step history. This also can be seen from the experimental data as shown in Figs. 4 and 5.
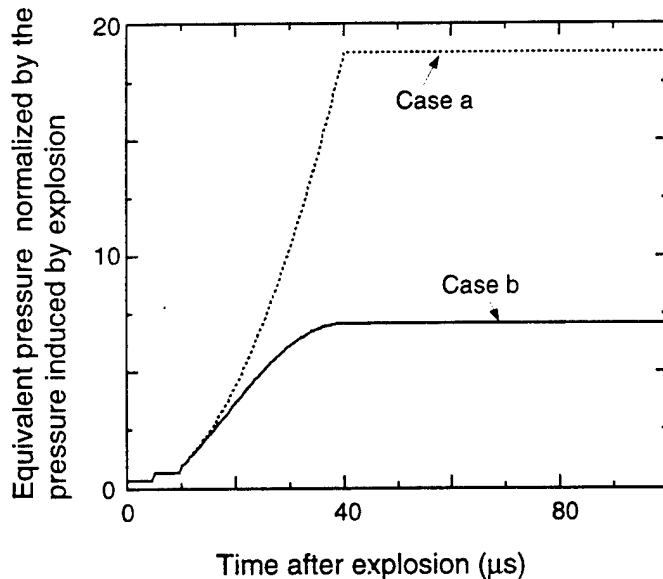
2. The cracking processes may play a very important role in the P-wave induced displacement history because radial cracking generated by the pressure in cavity and P-wave propagation changes the boundary conditions for the displacement field. When pressure in cavities is larger than some critical value, radial cracks are generated from inner surfaces. The radial cracks will make the tangential stress be either zero if the explosion products do not penetrate into cracks or the same pressure as in the cavity if the explosion products do penetrate into cracks. Whenever the explosion products penetrate into cracks, the tangential stress in rocks experiences a large change because the tangential stress goes from tensional, before cracking, to compressional, after cracking. These rapid changes give rise to shear waves. Radial cracking also generates P-waves because cracking is equivalent to increasing the effective cavity radius (a thin crack opening will not change the pressure in cavity very much).

Once the pressure starts to rise such that failure tension begins at time defined as, t_0, at time equal to t_{00} the pressure reaches a steady value. We assume rock fracture stops at this point. Two cases may be assumed (Fig. 8).

(1) Case a: crack velocity remains constant during crack propagation ($t_0 < t < t_{00}$)
(2) Case b: crack velocity decreases linearly with time during this interval.

Because the ratio of cavity radius to explosive radius is about 3, there is no separation between shock wave in air in the cavity and the adiabatic release wave of explosion products. The shock wave velocity in air can be estimated using the Chapman-Jourquet (CJ) theory. The particle velocity after the CJ detonation is

$$V_p = \frac{D}{\gamma + 1}, \qquad (9)$$

where D is CJ wave velocity.

For PETN, the typical CJ wave velocity is 8 km/s [Dobratz, 1974]. The particle velocity then is about 3.3 km/s. The vibration period in the cavity is

$$t_v \approx a/(2 * 3.3) \approx 2.3 \mu s \qquad (10)$$

From experimental data, the rise-time of the particle displacement induced by P-wave is ~ 10 µs, or, about three oscillation periods. This also can be verified from the profiles of the displacement rise-front from the experiments (e.g. see Figs. 4 and 5).

The maximum velocity of a mode-I crack is Rayleigh wave velocity [Freund and Clifton, 1974]. Compared to the crack velocity in rocks from seismology [Kanamori, 1994], the fault propagation velocity is ~70% of the theoretical maximum velocity of a mode-II crack, i.e., shear wave velocity. Crack propagation velocity, C^c, is assumed to be 70% of Rayleigh wave velocity, C_R, because the cracks generated in the experiments are both mode I and mode II.

Figure 8A shows the calculated results of displacement time history based on the pressure histories for Case a and Case b. The displacement history recorded from experiments lies between case a and b (curves b and c) of Fig. 8A. Thus cracks propagate neither at constant velocity nor at constant deceleration. From the comparison between the theoretical estimate based on Cases a and b and the experimental data, cracking process has very large effect on the history of displacement or strain. First, cracking processes increase the amplitude of low frequency component because cracking is equivalent to increase the volume of the cavity and hence pulse duration. Second, cracking processes increases the complexity of the directional dependence of displacement history because of nonuniform distribution of cracks.
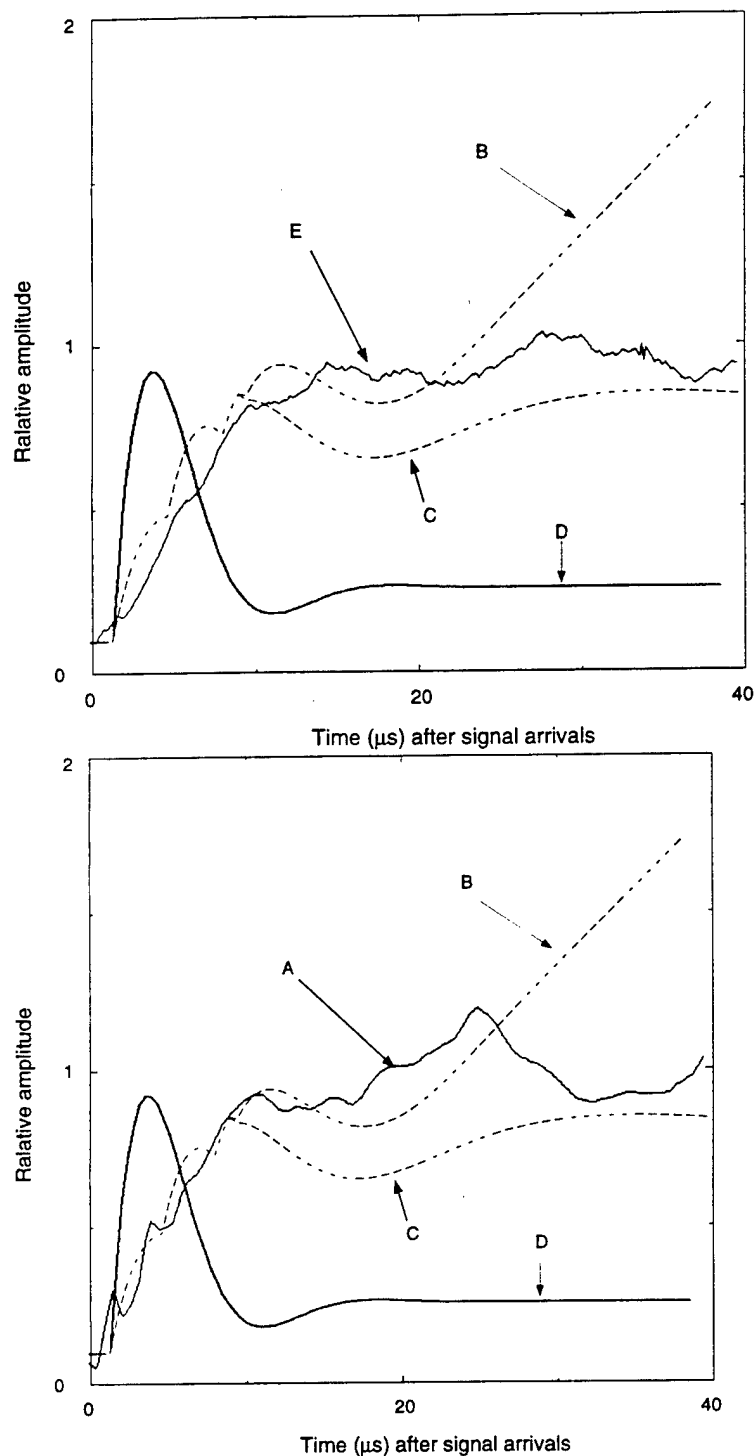
Fig. 8A. Comparison between experimental data and the results from different stress wave
models
A: Experimental data from shot SW4, gauge 2
B: Constant crack velocity model
C: Constant deceleration model
D: Constant step pressure model
E: Experimental data from Shot SW9, gauge 4

14

S-waves from explosions are generated from at least three different processes.
1. Micro-cracking.
2. Shock wave (P wave) to S conversion at the cavity wall.
3. Macro-cracking.
    In the case of each of these three sources, the arrival times of the S-waves from these sources can be approximately calculated.
    Fig. 9 shows the maximum strains from the gauges along direction 2 (Fig. 3) for shear waves generated from shock (compressional P-wave) wave-to-S-wave conversion and macro-cracking at different locations for Shot SW4 and SW9. Due to the difficulty to determine the actual S-wave incident angle at each gauge, two gauges at the same location (152 mm distance) are used to approximately determine the incident angle. Then the peak displacement of the S-wave from different generation mechanisms may tentatively be inferred as shown in Fig. 9. The procedure to determine S-wave incident angle using the two gauges at the same location is: (1) to find out the ratio of the strain from the gauge along direction 2 to the strain from the gauge along direction 1; (2) to calculate the incident angle. We note that this method is not very precise because P-waves interfere with S-waves but at least the method gives a first-order estimate of S-wave amplitudes induced by shock wave-to-S conversion at cavity wall and crack propagation in rock. Figure 10 shows the maximum displacement of S-waves at different distances from source. From this figure, it appears that the shear wave generated from shock wave-to-S conversion has a more systematic amplitude than the shear wave generated from macro-cracking.
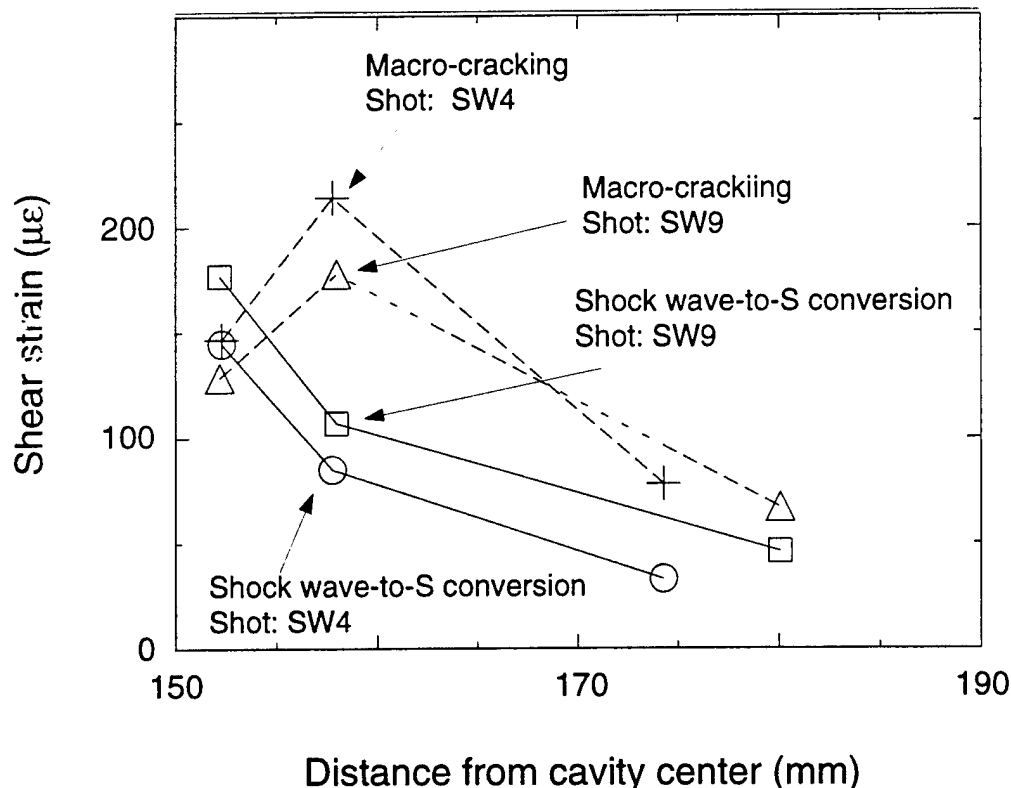

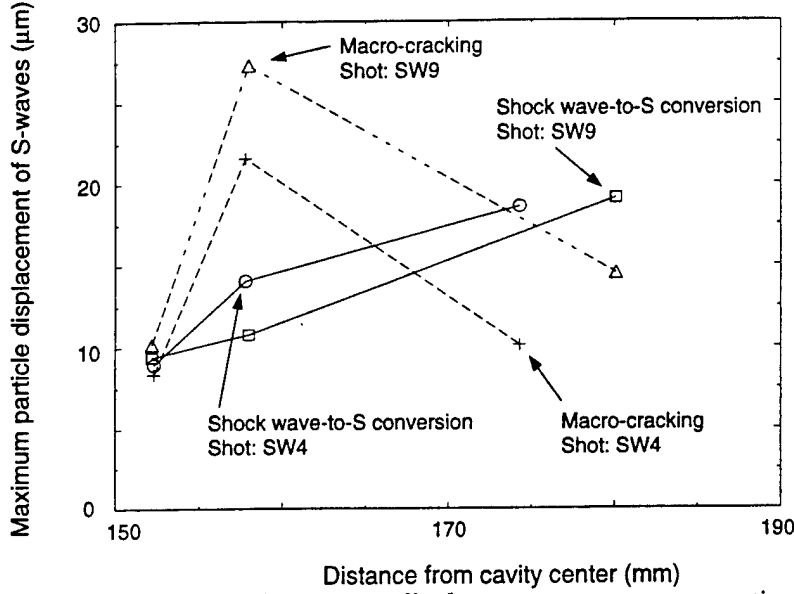Fig. 9. Maximum shear wave strain versus propagation distance.

Fig. 10. Maximum shear wave displacement versus propagation distance. Comparison of S-wave amplitudes produced by mode conversion and microcracking suggests the former is more predictable.

The S-wave amplitudes and profiles recorded by different gauges are dependent on the relative orientation of the gauges with respect to specific cracks (similar, in some respects, to the directivity of wave profiles in seismology).

Thus we expect to see that the S-wave profiles generated from cracking varies from gauge to gauge. In order to estimate the S-wave generated from cracking, we assume that the strain related with S-wave decay, varies with radial distance in a similar way as P-waves then

$$\varepsilon_s = \sum_i \varepsilon_{s_i}^0 \left(\frac{a_{ci}(t)}{r} \right)^{2.5}, \tag{11}$$

where $\varepsilon_{s_i}^0$ is the shear strain jump generated from the ith cracking at radius $a_{ci}(t)$, ε_s is the shear strain observed at r. The expression above means that the shear strain profile is controlled by the relative position of gauges with respect to each crack. In order to conduct an order-of-magnitude estimate of shear waves amplitude generated from cracks, we assume that this contribution is equivalent to a single crack and the crack propagates toward to the gauge. Then, the shear strain history can be estimated if we know the equivalent crack propagation velocity. Here, again we consider the two extreme conditions, i.e., crack propagation at constant velocity and at constant deceleration.

For constant velocity, the shear strain history is

$$\varepsilon_s = \varepsilon_{s_i}^0 ((a + C_0^c(t - t_0))/r)^{2.5} \tag{12}$$

where C_0^c is crack propagation velocity, a is the initial cavity radius and t_0 is the time required for crack to start propagating.

For constant deceleration model, the shear strain history is

$$\varepsilon_s = \varepsilon_{si}^0 ((a + C_0^c(t - t_0)) \frac{t_d + t_0 - t}{t_d})/r)^{2.5} \tag{13}$$

where t_d is time duration of crack propagation.

Based on the two equations above, the shear strain history is calculated as shown in Fig. 11 assuming that crack propagation times is similar for both modes (in order to compare these). In this figure, it appears that experimental results from gauge 3 for shots SW4 and SW9 and the results from the above model with the first part at constant velocity,

16

and the second portion of the source being approximated as a constant deceleration. It seems that a constant velocity source followed by a constant deceleration source fits the data reasonably well.
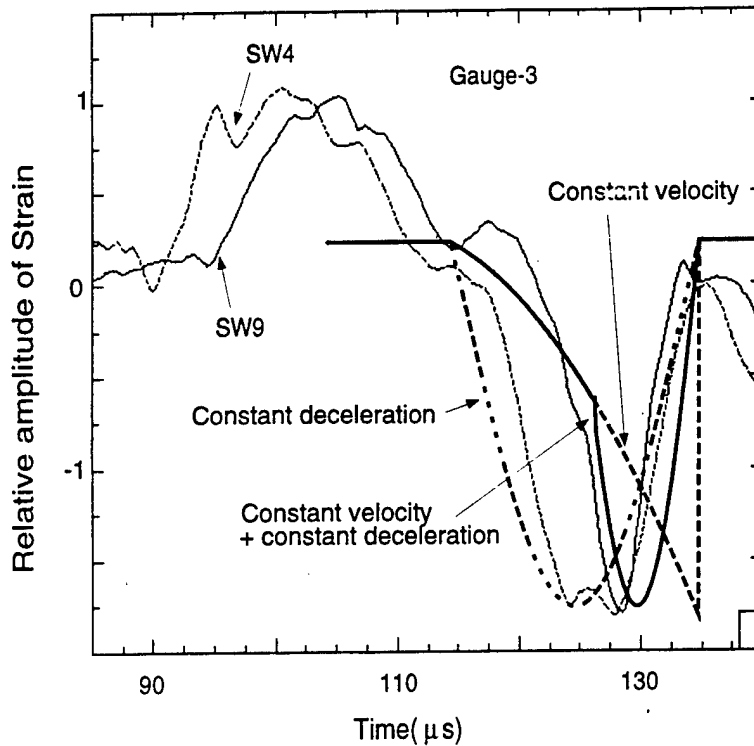

Fig. 11. Shear strain history recorded by Gauge #3 (see Fig. 3 for position) and shots SW4 and SW9 and deceleration predicted by the models of Fig. 8A..

Cracking induced by explosions in rocks is due to tensional failure. Thus the dynamical tensional strength controls the process. Rubin and Ahrens [1991] experimental data on the dynamic tensional strength of Bedford limestone showed that the tensional strength of Bedford limestone is very sensitive to pulse duration ($\sigma_f = 135$ MPa when the pulse duration is 0.3 μs and 58 MPa when the duration is 1.3 μs). In order to simply estimate the tensional strength under different wave durations, we assumed that the product of the tensional strength with the square root of the pulse duration, Δt, is a constant. From the experimental results [Rubin and Ahrens, 1991], the average $\sigma_f \sqrt{(\Delta t)}$ is 70 MPa $(\mu s)^{1/2}$. From the P-wave particle displacement profile as shown in Fig.12, the rise-time of the P-wave particle displacement is approximately 10 μs. The tensional strength of Bedford limestone for 10 μs-duration P-wave pulse, is therefore $\sigma_f \approx 22$ MPa. We note that initially the shear signal starts at T_{s1}, the interval ΔT_{s1} is due to tensile cracking whereas T_{s3e} to $T_{s3}\ell$ corresponds to mode P- to S-wave conversion.

In order to approximately estimate the S-wave amplitude, we assume that cracks are penny-shaped with final radius, R_0. The S-wave particle velocity, v_s, near crack surfaces can be estimated using

$$v_s = \frac{\varepsilon_{0f}}{\rho C_s} \qquad (14)$$

17

where $\rho = 2.42 \text{g/cm}^3$ and $C_s = 2.8$ km/s [Rubin and Ahrens, 1991] is the density and shear wave velocity of Bedford limestone, respectively. Then $v_s \approx 3.3$ m/s. The shear strain near crack surface is

$$\varepsilon_f \approx \frac{v_s}{C_s} = 0.0012 \tag{15}$$

Then the shear strain at a gauge position achieves a maximum value when crack stops propagating. Assuming the same decay as P-wave, the maximum shear strain recorded by gauge at radial distance, r, is

$$\varepsilon_s = \varepsilon_f \left(\frac{R_c}{r} \right)^{2.5}, \tag{16}$$

where R_c is the radius at which cracks stop. Based on the data used above, we have

$$\varepsilon_s \approx 0.0012 \left(\frac{50 + 15}{150} \right)^{2.5} \approx 150 \mu\varepsilon \tag{17}$$

From the experimental data, the maximum shear strain is from 50 $\mu\varepsilon$ to 180 $\mu\varepsilon$. The prediction is in good agreement with the experimental data.
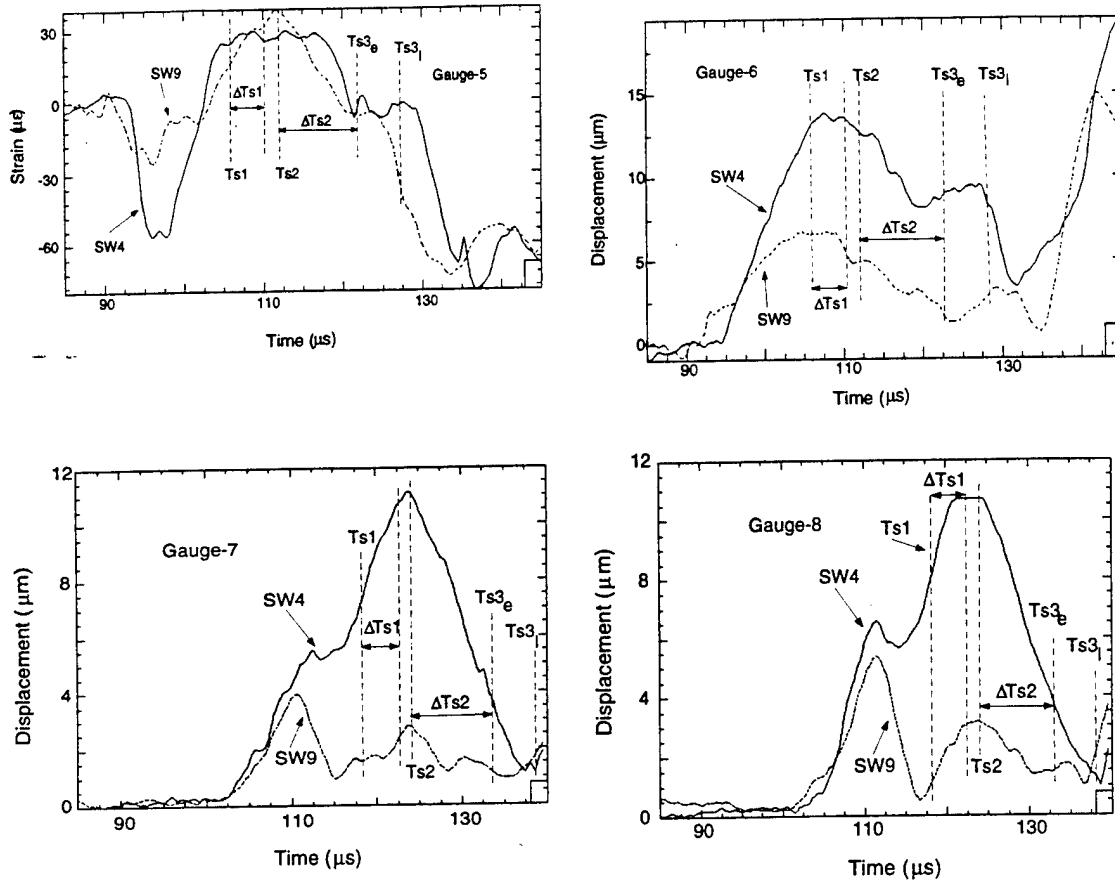

18
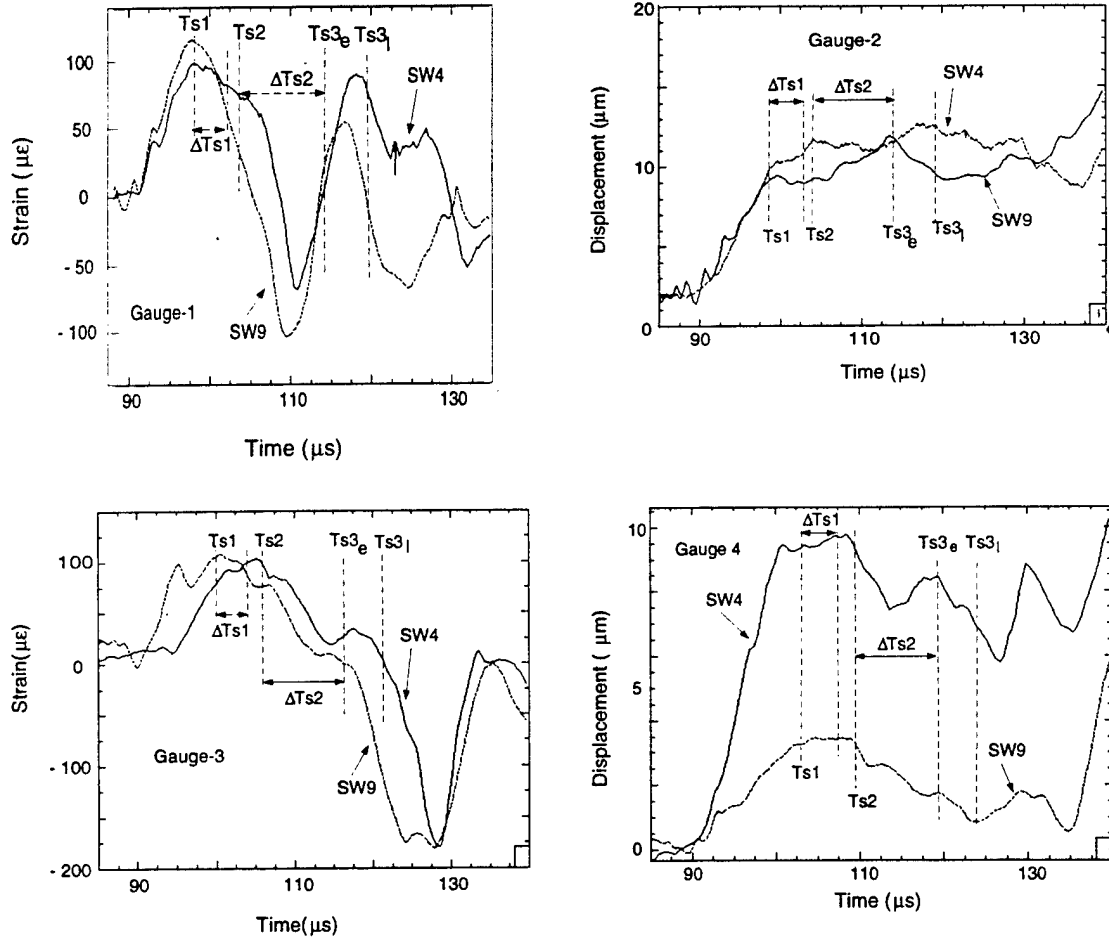
Fig. 12. Strain signals at gauge positions 1-8 for shots SW4 and SW9. Times T_{s1} and T_{s2} correspond to onset of macro-shear wave cracking converted, whereas T_{s3e} to T_{s3} ℓ correspond to mode-converted (on the cavity wall, mode conversion).

REFERENCES

Dobratz, B. M., Report, UCRL-51319, Lawrence Livermore National Laboratory, 1974.
Freund, L. B., and R. J. Clifton, On the uniqueness of plane elastodynamic solutions for running cracks, *J. of Elasticity*, *4*, 293-299, 1974.
Kanamori, H., Mechanics of earthquakes, *Annu. Rev. Earth Planet. Sci.*, *22*, 207-237, 1994.
Murphey, B. F., Particle motions near explosions in halite, *J. Geophys. Res.*, *66*, 947-958, 1961.
Rubin, A. M., and T. J. Ahrens, Dynamic tensile failure induced velocity deficits in rock, *Geophys. Res. Lett.*, *18*, 219-222, 1991.
Timoshenko, S. P., and J. N. Goodier, *Theory of Elasticity*, McGraw-Hill, New York, 1970.